Interactions of Anti-Inflammatory and Antibiotic Drugs at Mineral Surfaces Can Control Environmental Fate and Transport

Tao Luo, Jing Xu, Wei Cheng, Lian Zhou, Remi Marsac, Feng Wu, Jean-François Boily, Khalil Hanna

Interactions of anti-inflammatory and antibiotic drugs at mineral surfaces can control environmental fate and transport

Tao Luo[a], Jing Xu[b], Wei Cheng[c], Lian Zhou[a], Rémi Marsac[d], Feng Wu[e], Jean-François Boily[f], Khalil Hanna [a,g,*]

[a] Univ Rennes, Ecole Nationale Supérieure de Chimie de Rennes, CNRS, ISCR-UMR 6226, F-35000, Rennes, France.

[b] State Key Laboratory of Water Resources and Hydropower Engineering Science, Wuhan University, Wuhan 430072, P. R. China

[c] College of Resources and Environmental Science, South-Central University for Nationalities, Wuhan 430074, P. R. China

[d] Univ Rennes, CNRS, Géosciences Rennes – UMR 6118, F-35000 Rennes, France.

[e] Hubei Key Lab of Biomass Resource Chemistry and Environmental Biotechnology, School of Resources and Environmental Science, Wuhan University, Wuhan, 430079, P. R. China.

[f]Department of Chemistry, Umeå University, Umeå, SE-901 87, Sweden

[g]Institut Universitaire de France (IUF), MESRI, 1 rue Descartes, 75231 Paris, France.

*Corresponding author: Tel.: +33 2 23 23 80 27, khalil.hanna@ensc-rennes.fr

Abstract

Various pharmaceutical compounds often coexist in contaminated soils, yet little is known about how their interactions impact their mobility. We here show that two typical antibiotic and anti-inflammatory agents (nalidixic acid (NA) and niflumic acid (NFA)) commonly form dimers at several representative soil- and sediment-building minerals of contrasting composition and structure. Co-binding occurs in the form of a NFA-NA dimer stabilized by hydrogen bonding and van der Waals interactions. Using dynamic column experiments containing goethite-coated sand, we then demonstrated that pre-sorbed NA effectively captured the otherwise weakly-binding NFA from solution. Simultaneously injecting NA and NFA to pre-sorbed NA enhanced even further both NA and NFA loadings, thereby altering their transport under flow-through conditions. We also showed that environmental level amounts of natural organic matter can reduce the overall retention in column experiments, yet it does not suppress dimer formation. These environmentally relevant scenarios can be predicted using a new transport model that accounts for kinetics and co-binding reactions of NFA onto NA bound to goethite through metal bonded, hydrogen-bonded and an outer-sphere complexes. These findings have important implications on assessing the fate of co-existing pharmaceutical compounds under dynamic flow conditions in contaminated soils.

Keywords: pharmaceutical compounds; mobility; cooperative binding; transport; modeling.

Synopsis

This work contributes to efforts aiming to accurately assess co-binding mechanisms and the fate of co-existing contaminants in the environment.

Graphical Abstract

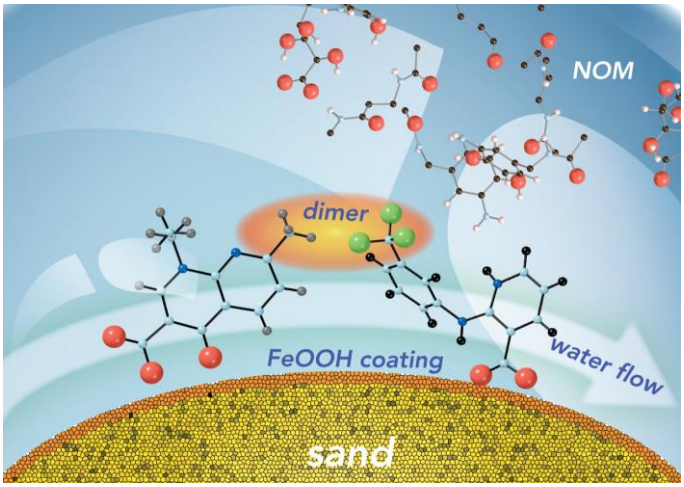

1. Introduction

Pharmaceutical and personal care products often co-exist in aquatic systems at levels as high as several hundred ng per L[1–4]. Recently, antibacterial and anti-inflammatory agents have emerged as aqueous micropollutants in surface waters, groundwaters and soils [2,5]. The transport and mobility of these emerging contaminants in the environment are strongly related to the nature and relative abundance of the mineral phases (*e.g.* metal oxides and clays) commonly found in the Earth's near-surface environment[6–8]. For this reason, several studies have focused on interactions of organic compounds with metal-oxyhydroxides and clays[8–12]. Still, much remains to be learned on their fate and transport mechanisms in oxide-rich environments, and particularly in multicomponent systems. In such systems, adsorption, through competitive or synergistic interactions at mineral surfaces, is key to determine the fate of pollutant mixtures[13–15].

Recent spectroscopic, chromatographic and theoretical investigations have improved the description of quinolones and fluoroquinolones adsorption to Fe-oxides by identifying ligands that are (i) metal-bonded (MB; inner-sphere (IS)), (ii) hydrogen-bonded (HB; direct H-bond to surface (hydr)oxo group) or (iii) bound as outer-sphere (OS; separated by at least one hydration sheath) species. The relative importance of these species is affected by pH, ionic strength, as well as mineral surface and ligand structures[16–19]. More particularly, we have shown that the spatial

disposition functional groups of niflumic acid (NFA, a non-steroidal anti-inflammatory) favor HB over MB species at goethite (α-FeOOH) surfaces over a broad range of pH values[18,19]. In contrast, the keto group and carboxylate groups of nalidixic acid (NA, a quinolone antibiotic) favor MB species. [19,20] Here, MB species dominate under acidic conditions, while HB/OS coexists under circumneutral to alkaline conditions.

Because most traditional environmental models are based on a single/individual contaminant basis, little is known on their transport in mixture contaminant systems, and underlying reaction mechanisms remain elusive. In addition, much of the knowledge that currently exists concerns the reactivity of environmental mineral surfaces in suspensions or slurry systems, and under equilibrium conditions[7,10,21–23]. Fewer investigations have been performed on the impact of water flow on the interfacial processes, and much less in flow-through system where non-equilibrium prevails. Moreover, non-equilibrium sorption under dynamic flow conditions is particularly relevant when competitive or cooperative process in presence or absence of natural organic matter (NOM) concurrently impact the mobility of target compounds[4,24,25].

In this work, we assessed the ability of NA and NFA to co-bind at minerals surfaces. To identify the mineralogical controls on NA and NFA co-binding we monitored their uptake by batch adsorption on seven nanominerals of contrasting

composition and structure (goethite, magnetite, hematite, gibbsite, kaolinite, bentonite and titanium dioxide). These natural constituents of soils and sediments are the most reactive minerals in the environment, and play an important role in controlling the fate, mobility and toxicity of contaminants. Then, to emulate contaminant migration in natural environments, such as in aquifers and sediments, we monitored NA and NFA transport in column experiments using goethite-coated quartz sand particles. Goethite, a widespread mineral in aquatic and terrestrial systems, is one of the most thermodynamically stable iron oxide with a high surface area[26]. Furthermore, goethite is often forming coatings on less soluble soil particles such as silica sand, and thus goethite-coated sand material is generally used as a structurally stable and hydraulically conductive porous medium to mimic natural mineral assemblages[27,28].

We compared NA and NFA binding (1) in isolated *vs.* mixed systems, and (2) in settings emulating stagnant *vs.* flowing groundwater containing Leonardite humic acid (LHA), a representative NOM. The NOM concentration range (5-10 mg/L) corresponds to the dissolved organic carbon typical of shallow groundwater, soil pore waters and surface waters[29,30]. Breakthrough curves (BTCs) of NA and NFA determined under different water velocities and residence times showed that co-binding of NA/NFA significantly altered the mobility of each compound. Although we have used an inflow concentration of NA or NFA higher than the level amounts of pharmaceuticals commonly detected in environmental systems (several hundred of ng per L)[1–4], previous experimental and computational quantum findings showed that the formation of NFA-NA dimer at the surface of AlO(OH) or FeO(OH), is

thermodynamically favorable, and can even occur for the very low concentration range[19]. In addition, dynamic breakthrough experiments provide a high solid-to-liquid ratio, *i.e.* a small volume flowing through the porous media in packed bed columns, and therefore a total contaminant loading more representative of environmental settings[17,18].

Multisite complexation model (MUSIC) was also established to describe the co-binding results of NA and NFA onto goethite, and predictions of BTC have been developed from surface complexation modeling parameters combined with a new kinetics term. This chemical kinetic/transport coupling was required to accurately describe the mobility of NA and NFA in the different scenarios considered in this study. These efforts helped identify conditions under which drug co-binding is likely to prevail in the environment, and highlight the importance of coupled flow and water chemistry in controlling the mobility of pharmaceutical compounds in complex environmental media.

2. Materials and Methods

2.1 Chemicals

Nalidixic acid (NA), Niflumic acid (NFA), ferric nitrate nonahydrate ($Fe(NO_3)_3 \cdot 9H_2O$), sodium chloride (NaCl), sodium hydroxide (NaOH), hydrochloric acid (HCl) and potassium bromide (KBr) were provided by Sigma Aldrich and were of analytical grade or better, and used without further purification. All solutions were prepared with ultrapure water. Leonardite Humic Acid Standard (1S104H) was

purchased from the International Humic Substance Society. A LHA stock solution (2 g/L, 1276 mg C/L) was prepared by dissolving 2 g LHA in 100 mL of 1 M NaOH, then diluted to 1 L with ultrapure water. Fontainebleau quartz sand (150-300 μm) was purchased from VWR Prolabo (France). Ultrapure water was used in all experiments.

2.2 Synthesis and characterization of minerals

Goethite, hematite, magnetite, gibbsite were synthesized using published methods, and described in the SI. Commercial TiO_2 Millennium PC-500 (> 99% of anatase), Georgia kaolinite (KGa-1) and Bentonite (Na-montmorillonite) were used as received. More information about synthesis and characterization are given in the Supporting information (SI).

Goethite coated sand (GCS) was obtained by mixing 500 g of Fontainebleau sand with an excess of goethite (~10 g) in 1L of 10 mM NaCl solution. Before coating, the quartz sand was cleaned with HCl, then with H_2O_2, and rinsed with pure water. The resulting goethite-sand suspension was adjusted to pH 5 and then shaken for 24 h. After that, the coated sand was washed with ultrapure water until the runoff was clear, and then it was dried in oven at 60°C for 24 h. The final GCS was stored at ambient temperature. Acid digestion followed by measurements of total dissolved iron using Inductively Coupled Plasma Atomic Emission Spectroscopy (ICP/AES), has permitted to determine the coating degree. For GCS, we found 0.9 g goethite per 100 g of coated sand. Previous studies from our group[17,20] confirmed that the coating

procedure did not alter the reactivity of goethite particles.

The possible dissolution of the used quartz sand was also checked in sand suspensions with two solid loadings, 1 or 10 g/L, aged for one month and at various equilibrium pH (4-10), in pure water or 0.01 M NaCl. In both cases were dissolved silicate concentrations below the detection limits of the molybdenum blue spectrophotometric method (detection limit 1µM) and of ICP/AES analyses (detection limit 0.2 µM)).

2.3 Batch experiments

Batch adsorption experiments were conducted in 10 mL suspensions of minerals in polypropylene tubes at a wide range of pH and in 10 mM NaCl to assess the NA/NFA co-binding on different types of minerals. The investigated pH range was adapted for each mineral to avoid mineral dissolution at very low or high pH values. All experiments were carried out under an atmosphere of N_2(g) in order to avoid contributions from dissolved CO_2. Suspensions were mixed for a period of 24 h by end-over-end shaking, which is largely sufficient to reach equilibrium based on preliminary kinetic study[18]. Aliquots of the resulting suspensions were thereafter sampled and filtered (0.2 µm) for analysis. NA and NFA co-binding to goethite were also investigated at pH 5 ± 0.1 in presence of various LHA concentrations. All batch adsorption experiments were performed in triplicates, with a reproducibility of 5 % for NA and 7 % for NFA. Results for the LHA-free systems are in the SI only.

NA and NFA concentrations in the aqueous solution were determined using a high performance liquid chromatography (HPLC) system. This was equipped with an auto sampler (Waters 717 plus) using a C18 column (250 mm×4.6 mm i.d., 5 μm), and a UV detector operating at 258 nm and 283 nm (Waters UV). The mobile phase was a mixture of water/acetonitrile (60:40 v/v) containing 0.1% of formic acid. The flow rate of the mobile phase was set at 1 mL/min in isocratic mode.

2.4 Continuous flow experiments

Breakthrough column experiments were conducted in a glass chromatographic column (1.6 cm internal diameter). The porous bed had a length of 4.9 cm and a dry mass of 15 g. After packing to a uniform bulk density (1.52 g/cm^3), the column was wetted upward with a background electrolyte solution (NaCl, 10 mM) at a constant flow rate for at least 24 h until the column was saturated and each parameter (pH, conductivity) became constant. After water saturation, 1 pore volume of 10 mM KBr (with 10 mM NaCl, pH 5) was injected in between the NaCl background solution to determine the flow characteristics of the porous bed. The tracer BTC was recorded by ion chromatography (Fig. S1 in supporting information, SI). The classical convection dispersion equation (CDE) was applied to describe the 1D transport of a non-reactive solute under steady-state water flow in a saturated column (*cf.* SI for detailed description of model). The fitting parameters of the bromide elution confirmed the flow homogeneity and predominance of a convective regime in the column. The mass balance ratios calculated based on BTCs of Br^- were close to 100% (Fig.

S1). The hydrodynamic parameters estimated includes total water content θ (0.36±0.005) and dispersivity λ (242 ± 2 μm) (See SI).

After the pulse tracer experiments, four sets of column experiments were performed by step-injection at the same constant flow rate of : (i) NFA/(NA+NFA): injection of 10 μM of NFA first, then 10 μM NA+10 μM NFA when the total breakthrough of NFA was achieved; (ii) NA/(NA+NFA): injection of 10 μM of NA first, then 10 μM NA+10 μM NFA when the total breakthrough of NA was achieved, (iii) (NA+NFA): simultaneous injection of 10 μM NA+10 μM NFA directly; (iv) (NA+NFA+LHA): simultaneous injection of 10 μM NA+10 μM NFA + 5/10 mg/L LHA. In all four approaches, influent solutions were prepared at pH_{in} 5 ± 0.1 and contained 10 mM of NaCl. Continuous on-line pH measurement was performed using pre-calibrated pH flow through sensor. In addition, the pH of collected fractions was often checked using a pH-meter (HI2210, HANNA®). The breakthrough curves (BTCs) were expressed as the relative aqueous concentration of solute against the number of pore volumes (V/V_p), where V_p represents the pore volume of column. The adsorbed amounts of NA and NFA were determined by integrating the area above the entire breakthrough curve of each compound, as previously reported[28,31]. The mass balance was further confirmed by carrying out solid-phase extraction on GCS, as described in previous work[32]. Briefly, the solid from packed column was transferred into an aqueous solution and then pH was adjusted to 11, and the suspension was stirred for 1h. The average extraction recovery derived from several desorption tests

lied at 97.9 ± 3.5%, confirming that only adsorption took place in the GCS column, and that molecule breakdown by, for example, oxidation, did not occur under the experimental conditions of this study. The aqueous concentrations of NA and/or NFA in the outflow were determined by HPLC. In all the column experiments, the leaching iron from GCS column was negligible. All experiments were conducted in duplicates, and the estimated error lied at 5% for NA and NFA.

2.5. Surface complexation modeling combined with kinetics

A surface complexation model (SCM) was used to predict adsorption under equilibrium condition. However, non-equilibrium may predominate in the dynamic column experiments, and thus implementation of kinetics in surface complexation reactions is crucial to accurately describe the mobility behavior. It was reported that a fast formation of outer sphere complexes is a prerequisite for inner sphere (IS) complexes formation, which is a rate-limiting process[33,34]. According to a previous spectroscopic study[34] showing that the conversion of hydrogen-bonded organic species to MB complexes was time-dependent, HB and OS complexes can be considered as intermediate species in our proposed conceptual model. To integrate kinetics in out SCM, we assume surface complexation reactions occur in two steps: (i) formation of precursor surface species (fast intermediate step) and (ii) formation of final surface species (rate-limiting step). According to our previous spectroscopic and theoretical investigations [18,19], NA can form (i) MB surface complexes *via* a NA keto group and one oxygen of the carboxylate group, (ii) HB complexes (surface

hydration-shared ion pair) and (iii) OS complexes (solvent-surface hydration-separated ion pair, where NA keeps its first hydration sphere) as follows:

$$2H^+ + 2{\equiv}FeOH^{-0.5} + NA^- \rightleftharpoons ({\equiv}FeOH_2)_2^+\cdots NA^- \quad (OS) \qquad (1)$$

$$2H^+ + 2{\equiv}FeOH^{-0.5} + NA^- \rightleftharpoons ({\equiv}FeOH_2)_2^+\cdots NA^- \quad (HB) \qquad (2)$$

$$2H^+ + 2{\equiv}FeOH^{-0.5} + NA^- \rightleftharpoons ({\equiv}Fe)_2(NA^0)+2H_2O \quad (MB) \qquad (3)$$

All modeling parameters are provided in Table S2.

To distinguish the two-step reactions in PHREEQC-2, we have applied the previously published approach[35]. Briefly, we defined one intermediate ('in') 'NA^{in}' and one equilibrium 'NA' species. Here, 'NA^{in}' is an intermediate complex first in the form of a OS species:

$$2H^+ + 2{\equiv}FeOH^{-0.5} + NA^{in-} \rightleftharpoons ({\equiv}FeOH_2)_2^+\cdots NA^{in-} \quad (OS\ formation) \qquad (4)$$

This OS species then converts to a HB species:

$$({\equiv}FeOH_2)_2^+\cdots NA^{in-} \quad (OS) \rightleftharpoons ({\equiv}FeOH_2)_2^+\cdots NA^{in-} \quad (HB\ formation) \qquad (5)$$

This conversion is a fast process, whereas the resulting HB species converts to a MB species through the following rate-limiting process:

$$({\equiv}FeOH_2)_2^+\cdots NA^{in-} \quad (HB) \underset{K_b}{\overset{K_f}{\rightleftharpoons}} ({\equiv}Fe)_2(NA^0) + 2H_2O \ (MB\ formation) \qquad (6)$$

Here, k_f and k_b are forward and backward rate coefficients (T^{-1}) respectively, which could be obtained by curve fitting, as previously reported.[35,36]. Preliminary fitting procedures allowed us to set forward rate constant k_f and backward rate constant k_b to 0.050 and 0.009, respectively.

The three plane model (TPM) was employed to describe the charge of the goethite/water interface, which requires two capacitances for the 0-(C_1 = 2.3 F/m^2) and the 1-plane (C_2 = 1.07 F/m^2). Then multi-site complexation (MUSIC) model and PHREEQC-2 was used for modelling the species transport in the GCS-packed column. Though singly ($\equiv FeOH^{-0.5}$), doubly ($\equiv Fe_2OH$) and triply ($\equiv Fe_3O^{-0.5}$ and $\equiv Fe_3OH^{+0.5}$) coordinated oxygens exist at the goethite surface, we assumed that NA and NFA trend to bind to reactive $\equiv FeOH^{-0.5}$ sites of goethite through HB, OS and even MB (only for NA) complexes based on our studies[18,19]. The reactive site density is given as detailed in our previous work: [$\equiv FeOH^{-0.5}$] = 3.12 sites/nm² and [$\equiv Fe_3O^{-0.5}$] = 3.12 sites/nm² on (001)/(101) planes (90% of the surface area), and [$\equiv FeOH^{-0.5}$] = 7.4 sites/nm² on (210)/(010) plane (10% of the surface area).

Our modeling strategy is described as follows. Surface hydrolysis and surface complexation reactions including NA/NFA dimer formation were taken from our previous batch sorption study[18]. For the column system, NA and NFA adsorption were first modeled in their respective single systems. The corresponding surface complexation constants were then used to predict binding in the binary system, and the NA-NFA dimer formation constant was calibrated from the experimental data. The column system was described by 1D transport, with p successive equal width cells ($\Delta z = L/p$, L is the total column length, in this study p = 20). Solution transported between p_n and p_{n+1} in time steps Δt and at the defined flow rate and dispersion through the

312 specific transport procedure implemented into PHREEQC-2. After each time step, this
313 procedure is coupled with the geochemical code for each cell[37]. All parameters used
314 for transport modeling are provided in Table S2.
315

316 # 3. Results and discussion

317 Our previous works[18,19] showed that enhancement in NFA binding, which is
318 otherwise considerable weaker than NA, results from the intermolecular interactions
319 with the goethite-bound NA. We ascribed this enhancement to a NFA-NA dimer
320 whose energetically favored formation (-0.5 eV compared to free molecules) is
321 predominantly driven by van der Waals interactions[19]. For reference, at pH 5, which
322 will be focused in our transport work, NA loadings on goethite (0.33 μmol/m^2; 0.20
323 NA/nm^2) are more than 3 times larger than NFA (~0.10 μmol/m^2; 0.06 NFA/nm^2) (Fig.
324 S2). Dimer formation in mixed NA and NFA solutions can enhance, in turn, NFA
325 loadings by a factor of ~2.5 (~0.10 $\rightarrow$ ~0.25 μmol/m^2) and NA loadings by ~1.2 (0.33
326 $\rightarrow$ ~0.40 μmol/m^2) (Fig. S2).
327

328 Comparison of this enhancement effect with a suite of other minerals (SI) of
329 contrasting composition and structure shows that NFA binding in the binary system
330 was greatest on goethite. Namely, it followed the order: goethite (2.5-fold) > TiO_2
331 (2-fold) > magnetite (1.8-fold) > gibbsite (1.5-fold, pH 6) ≈ kaolinite (1.5-fold) >
332 bentonite (1.3-fold) ≈ hematite (1.3-fold). See the SI for a more detailed discussions
333 of these results where we explain that NA-NFA dimer formation is greater on

nanominerals typically with homogeneous distributions of reactive –OH functional groups (goethite, TiO_2, magnetite), than those typically, with –OH limited to edges of platy minerals with unreactive basal faces (kaolinite, bentonite, hematite). For this reason, we focused our work on the effects of water flow and natural organic matter on NA-NFA interactions using goethite.

3.1. NA-NFA dimer formation under water flow

To explore the propensity of NA-NFA dimer formation under flow-through conditions, we performed dynamic flow experiments (Figs. 1, and 2) with columns filled with goethite-coated sand (GCS). First, we find that injection of a mixed solution of NA+NFA after *total breakthrough of NFA* (Fig. 1a) decreased NFA outlet concentrations due to NA-NFA dimer formation on the goethite surface. This started at ~27 V/V_p, reached a plateau at ~29.5 V/V_p, then it gradually increased to a complete breakthrough at ~1200 V/V_p. In contrast, injecting a mixed solution of NA+NFA after *total breakthrough of NA* (Fig. 1b) pushed the breakthrough point of NFA to ~25 V/V_p (insert of Fig. 1b) compared to 2.3 V/V_p in the single system (Fig. S3). The BTC of NFA then tailed extensively before reaching a total breakthrough, thus adopting a classical sigmoidal shape akin to that of NA. Here, NA loadings increased from 0.68 μmol/m^2 in the single system to 0.90 μmol/m^2 in the binary system (Fig. S4), a consequence of the pre-loaded NFA (Fig. 1). Simultaneously injecting NA and NFA after total breakthrough of NA increased both NA and NFA loadings (0.90 μmol NA/m^2; 0.33 μmol NFA/m^2), however at levels close to the

values obtained where NFA was first injected (Fig. 1). As a result, we find that NA and NFA exert a mutual effect on their breakthrough behavior under flow and this is basically explained from NA-NFA dimer formation at the goethite surface.

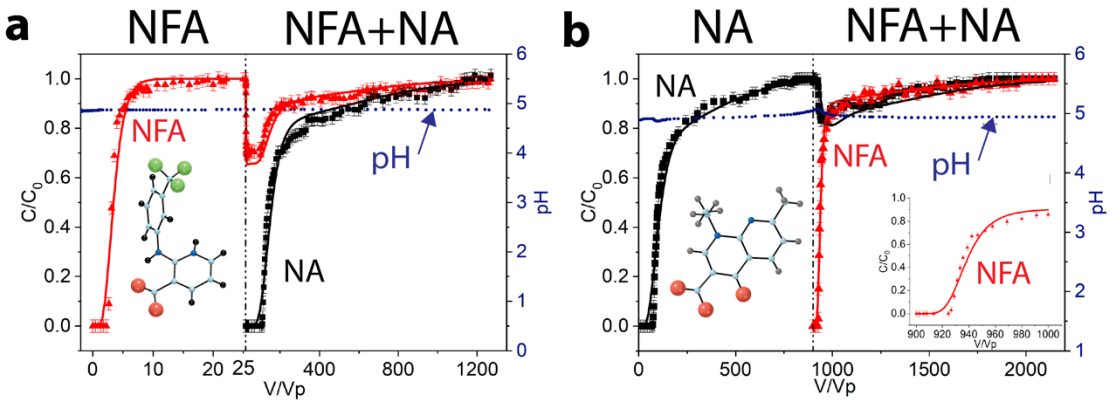

Figure 1. The full range of experimental breakthrough curves of NA and NFA through GCS-packed column in two successive steps at constant flow rate (0.5 ml/min). (a) Step I: injection of 10 µM NFA and 10 mM NaCl at pH_{in} 5 ± 0.1 until the complete breakthrough of NFA. Step II: injection of mixture of 10 µM NA + 10 µM NFA and 10 mM NaCl at pH_{in} 5 ± 0.1. The solid lines represent modelling results. (b) Step I: injection of 10 µM NA and 10 mM NaCl at pH_{in} 5 ± 0.1 until the complete breakthrough of NA. Step II: injection of mixture of 10 µM NA + 10 µM NFA and 10 mM NaCl at pH_{in} 5 ± 0.1. Insert is the breakthrough curve of NFA in the initial stage. The solid lines represent modelling results.

Irrespective of the injection scenario, NA exhibits an extended tailing suggesting kinetic limitations under the experimental conditions of this study. Because all of our bromide tracer experiments (Figs. S1 and S5) were well described using the CDE model, the tailing could not be explained by physical non-equilibrium effects, water regionalization into mobile/immobile zones or diffusion limitations between two water zones[38,39]. Moreover, the BTCs of NA and NFA in single systems were compared by normalizing the curves by their retardation factor to that of the bromide

tracer (Fig. S6). For NFA, the steepness of BTC showed coincidence with that of bromide, and only a short tail was observed. However, the normalized BTC of NA exhibits a significant difference in steepness and shape with respect to that of bromide. This discrepancy suggests the occurrence of chemical kinetic limitations or rate-controlled sorption processes under flow-through conditions. This is particularly the case for transport of the more strongly binding NA. This was confirmed further by results (Fig. S7) revealing greater NA loadings under conditions of lower flow rate (0.1 mL/min) that promotes higher residence times.

To check for the occurrence of kinetic limitations, SCM modeling with or without kinetics were compared for the BTC of NA (Fig. S8). These results confirmed that only kinetics implemented with SCM could describe the mobility behavior. In contrast, the equilibrium SCM seems sufficient for NFA, likely because of weaker and faster adsorption of NFA mainly through HB and OS complexes[18] (the first stage of Fig. 1a). However, as NFA adsorption on goethite was strongly related to kinetically limited NA adsorption, an extended tailing of NFA in the second stage was observed. As only the sorption kinetics of NA were considered here, we anticipate that this could affect the adsorption of NFA through co-binding reactions (*cf.* Table S2). Under such conditions, our combined SCM and kinetics reproduced the mobility of both NA and NFA (Fig. 1).

To provide further evidence for the co-dependency of NA and NFA binding to

399 GCS, we investigate the transport of the compounds under conditions where both NA
400 and NFA were injected simultaneously (Fig. 2) to a clean column. This revealed
401 two-step breakthrough behavior in the form of two fronts and of two plateaus in the
402 outlet concentration of NFA. This contrasts with the cases of where NFA was injected
403 before (Fig. 1a) or simultaneously with NA (Fig. 2). NFA sorption in the binary
404 system increased sharply to 0.34 μmol/m^2, compared to that in the single system, yet,
405 they still kept the same breakthrough point at 2.3 V/Vp (insert of Fig. 2). In
406 conclusion, although NA and NFA adopted contrasting BTCs from different injection
407 schemes (NFA/(NFA+NA), NA/(NFA+NA), and (NFA+NA)), their surface loadings
408 after total breakthrough were largely comparable (see Table S3). Here, NA and NFA
409 loadings both increased in the binary compound systems, 1.3 times for NA and 16-19
410 times for NFA compared to the single system. As such, although NA and NFA
411 transport processes depend on the injection methodology, because of the high-affinity
412 NA to goethite, the injection order has almost no effect on NA and NFA loadings and
413 in the co-binding behavior in the binary systems.
414
415 Finally, we confirmed these co-binding effects in experiments conducted at a
416 lower flow rate (0.1 mL/min; Fig. S7), where an extended tailing for NA or NFA was
417 also revealed. As a result, the same model previously used in sequential injection has
418 adequately described the behavior of NA and NFA in simultaneous injection approach
419 (Fig. 2).

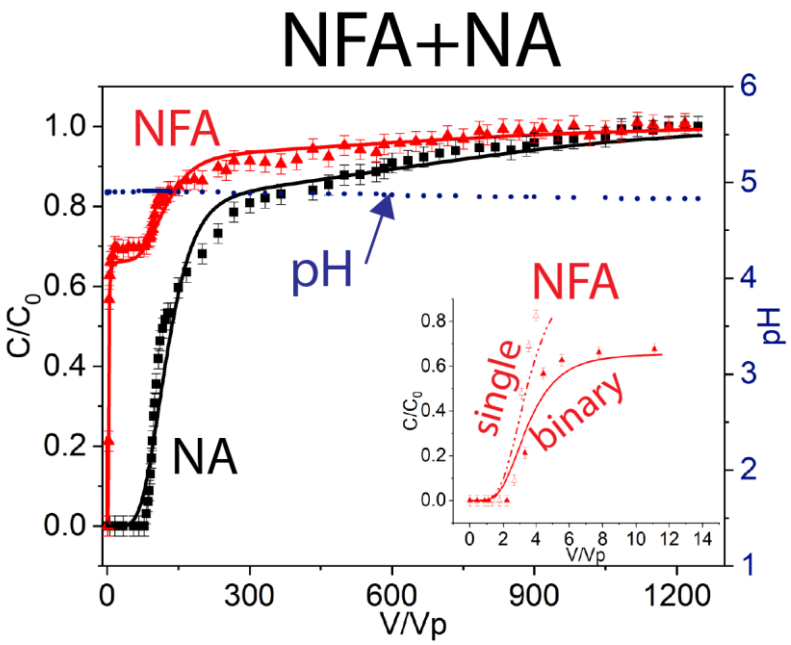

Figure 2. Experimental and calculated breakthrough curves of NA and NFA in binary system at flow rate of 0.5 mL/min through GCS-packed column. Inflowing solution contains mixture of 10 μM NA and 10 μM NFA 10 and 10 mM NaCl at pH_{in} = 5 ± 0.1. Insert is the breakthrough curves of NFA in the initial stage. The solid lines represent modelling results.

3.2 Altered fate of NA and NFA transport by natural organic matter

Building upon these results, we evaluated how NOM altered the fate of NA and NFA interactions. We used LHA as a representative NOM at loadings of up to ~ 1 mg C/m^2 (~ 50 C atoms/nm^2) at pH 5 on goethite. From batch adsorption experiments (Fig. 3) we find that LHA binding effectively decreased, yet did not completely suppress, NA loadings. At the same time, we find that LHA fully suppressed NFA co-binding at LHA loadings above ~ 0.2 mg C/m^2 (~10 C/nm^2). Based on previous work from our group[40], the goethite surface still exposed unreacted −OH groups at this loading, and is therefore not entirely covered by LHA. Still, bound LHA was

sufficiently effective to prevent binding NFA to the near-interfacial region of goethite for NA/NFA dimer formation. One possible explanation is that LHA altered the interfacial hydration environment and the surface charge of goethite, and thus the potential energy landscape for the NFA diffusion across the goethite/water interface and onto goethite-bound NA. It is also interesting to note that LHA offer no possibilities for NFA binding via, for example, van der Waals π–π electron coupling interactions. The enhanced uptake of NFA with NA is therefore driven by a very specific steric control between these two molecules.

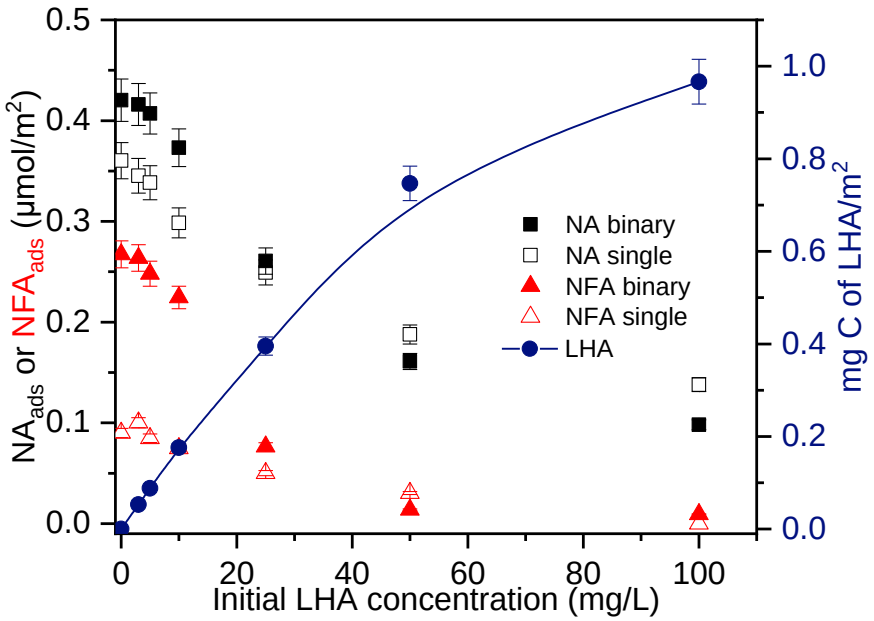

Figure 3. The effect of humic acid on the adsorption of NA and NFA on 0.5 g/L goethite in single ([NA]tot = 20 µM or [NFA]tot = 20 µM) and binary ([NA]tot = [NFA]tot = 20 µM) system at pH 5 and ionic strength 10 mM (NaCl).

Experiments under flow (Fig. 4), again using GCS, showed that LHA at two environmentally-relevant concentrations for groundwater and surface waters[29,30] (5 and 10 mg/L) also affected NA and NFA mobility. Despite the competitive binding

with LHA, co-binding and a two-step breakthrough behavior were still observed (Fig. 4a,b). Small breakthrough times and shorter tailing (steeper BTC) likely resulted from the consumption of adsorption sites by LHA. At relatively low LHA loadings, both NA and LHA compounds bound to goethite surface sites through ligand-exchange and hydrogen bonding, in turn altering the breakthrough behavior of NA. This competitive binding between NA and carboxylic/aromatics compounds of LHA may occur at the first step, followed probably by further adsorption of NA to LHA covered goethite. NFA enhanced adsorption could be clearly observed (from 0.02 to 0.17 μmol/m^2 at 5 mg/L LHA), though this increase was reduced with increasing in LHA amount (from 0.02 to 0.04 μmol/m^2 at 10 mg/L LHA), likely because of the decrease in NA sorption as a result from LHA competitive binding (*cf.* Table S3).

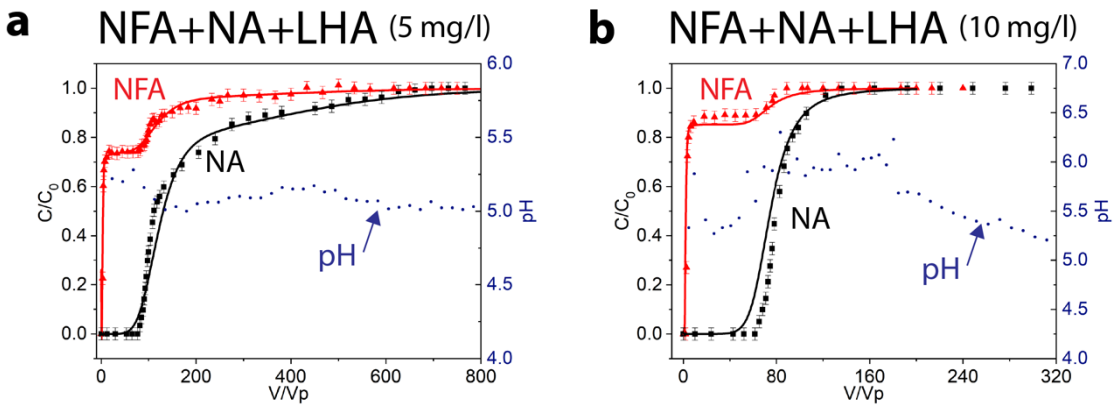

Figure 4. Experimental and calculated breakthrough curves of NA and NFA in multicomponent system with LHA at flow rate of 0.5 mL/min through GCS-packed column. a) Inflowing solution contains mixture of 10 μM NA, 10 μM NFA and 5 mg/L of LHA and 10 mM NaCl at pH_{in} = 5 ± 0.1. b) Inflowing solution contains mixture of 10 μM NA, 10 μM NFA and 10 mg/L of LHA and 10 mM NaCl at pH_{in} = 5 ± 0.1. The solid lines represent modelling results.

473 Based on previous studies[20,41,42] we can expect that LHA binding results in a
474 molecular fractionation caused by selective adsorption of heterogeneous LHA
475 components. Lower molecular weight fractions of LHA with higher aromaticity could
476 have primarily, and preferentially, bound to goethite in the first adsorption stage[42].
477 The higher molecular weight fractions, such as lignin-like and aliphatic compounds,
478 could have, in turn, bound in the following stage[42]. This view falls in line with the
479 breakthrough behavior of LHA in GCS column, particularly in terms of the
480 discrepancy between TOC and UV, which we report in Fig. S9 of the SI. In essence,
481 higher TOC values with respect to UV absorbance at 254 nm were observed during
482 the first adsorption stage. This aligns with the concept that LHA compounds of
483 smaller molecular weight were preferentially adsorbed and successively replaced
484 those of higher weight, as previously reported [37]. The same behavior was previously
485 observed when only LHA was injected in GCS column[20], suggesting that the presence
486 of NA and NFA did not significantly affect the binding of LHA components in
487 column.
488
489 As NOM consists of a polydisperse mixture of organic molecules of varying
490 molecular size, incorporation of complex binding reactions of the LHA components in
491 TLM model is not straightforward. To simplify the model, we only considered sites
492 consumed by LHA components. Then we reduced the available goethite site density
493 (*i.e.* 15 % reduction for 5 mg/L LHA; 60% reduction for 10 mg/L LHA) to describe
494 the modification of NA and NFA BTC in presence of LHA. These results could

suggest that changes in site density were not linearly correlated to LHA loadings, and this could be explained by LHA fractionation and complex interactions with goethite. We have also slightly adjusted the surface NA-NFA dimer formation constant of NA and NFA (Table S2) (24.4 → 23.8 for 5 mg/L LHA; 24.4 → 23 for 10 mg/L LHA) to improve the fit to the data, as the presence of LHA likely alters the formation of NA-NFA dimer. Because of the functional (*e.g.* carboxylates) groups of LHA, the complexation constant of NA on goethite by HB (Table S2) was also modified (20.4 → 20.6 for 5 mg/L LHA; 20.4 → 21 for 10 mg/L LHA). These slight adjustments improved the fit of our model to the experimental data (Fig. 4), and thus our ability to predict multicomponent transport in complex systems. This consequently adds further confidence to the ability of our proposed model to account for NA and NFA (co)-binding under real-world conditions.

Environmental implications for environmental fate of pollutant mixtures

Emerging contaminants such as pharmaceutical compounds in the environment often occur in mixtures rather than as individual entities. The increasing occurrence of multiply contaminated aquatic ecosystems worldwide require efforts to predict synergistic and antagonistic effects affecting the transport of toxic agents in nature.

This study contributes to mounting evidence showing that mobility of pollutant mixtures cannot be predicted based on single-compound based adsorption data. More particularly, we showed that mineral-bound antibiotics can be new adsorption sites for

other contaminants at mineral surfaces. Since this cooperative phenomenon is strongly dependent on the molecular structure of target compound (*e.g.*, possibility of Van der Waals interactions and/or hydrogen bonding), it cannot be generalizable to all pharmaceutical compounds. Indeed, a parallel set of efforts showed that no co-binding occurred with sulfamethoxazole (SMX) neither with NA nor NFA, because of the lack of molecular interactions of SMX with co-existing compounds and goethite surfaces. In contrast, ciprofloxacin (CIP) containing carboxyl and carbonyl functional groups, enhanced NFA binding, because CIP strongly binds to goethite surfaces, and may act as an attachment site for NFA. Therefore, this work raises the importance of recognizing drug co-binding, and lack of co-binding, for accurately predicting the fate of complex pharmaceutical mixtures in the environment.

Flow-through column experiments showed that co-binding caused by intermolecular interactions considerably affects the mobility and transport of NA and NFA in reactive porous media. These new findings combined with batch data and previous theoretical calculations[19] confirmed that the co-binding phenomenon takes place at the mineral surface, and over a wide range of aqueous concentration. Though the concentration in inflow solution may appear higher than the level of aqueous concentration commonly found in aquatic systems[1–5], continuous flow-through conditions offered the possibility to work with a suitable soil-aqueous phase ratio, and then monitor the effects of dispersion and nonequilibrium sorption on the transport of pollutants. This would certainly bring dynamic-flow tests closer to environmental and real-world conditions.

539 The presence of environmental level amounts of natural organic matter can
540 reduce the overall retention by minerals, yet it does not suppress cooperative binding.
541 Taking these phenomena into account in a new SCM, which even accounts for kinetic
542 effects, allowed us to predict cooperative adsorption under dynamic flow and
543 non-equilibrium conditions. This new transport model has the potential of
544 successfully predicting the fate of pharmaceutical compounds, as NA and NFA, in
545 various different environmentally relevant scenarios, and over a wide range of
546 concentration including the level amounts commonly detected in environmental
547 systems.

548 As these co-binding mechanisms at mineral surfaces are not often considered in
549 traditional thermodynamic modeling, our findings raise the importance of recognizing
550 co-binding as a mechanism contributing to the migration of antibiotics and
551 anti-inflammatory agents in complex environmental mixtures. As such, this work
552 contributes to efforts aiming to accurately assess co-binding mechanisms at
553 environmental surfaces, and the fate of co-existing contaminants in the environment.

554

555 **Supporting Information.** Synthesis and characterization of minerals; tracer
556 experiments and modeling; co-binding of NA and NFA on different nanominerals;
557 experimental BTCs of NA or NFA with different flow rates and calculated BTCs of
558 NA by using equilibrium and kinetic model in PHREEQC-2**.** Breakthrough curves of
559 LHA at 5 and 10 mg/L.

560

561 **Acknowledgements**

562 This work was supported by the Institut Universitaire de France, the Swedish
563 Research Council (2020-04853), the French National Research Agency via the
564 C-FACTOR project (ANR-18-CE01-0008) and the CNRS (PICS 2018-2020). We
565 gratefully acknowledge the Chinese Scholarship Council of PR China for providing
566 financial support for Tao Luo to stay at the ENSCR.

567

References

(1) Fatta-Kassinos, D.; Meric, S.; Nikolaou, A. Pharmaceutical Residues in Environmental Waters and Wastewater: Current State of Knowledge and Future Research. *Anal. Bioanal. Chem.* **2011**, *399* (1), 251–275.

(2) Dębska, J.; Kot-Wasik, A.; Namieśnik, J. Fate and Analysis of Pharmaceutical Residues in the Aquatic Environment. *Crit. Rev. Anal. Chem.* **2004**, *34* (1), 51–67.

(3) Heberer, T. Occurrence, Fate, and Removal of Pharmaceutical Residues in the Aquatic Environment: A Review of Recent Research Data. *Toxicol. Lett.* **2002**, *131* (1), 5–17.

(4) Wu, Q.; Li, Z.; Hong, H. Adsorption of the Quinolone Antibiotic Nalidixic Acid onto Montmorillonite and Kaolinite. *Appl. Clay Sci.* **2013**, *74*, 66–73.

(5) Khetan, S. K.; Collins, T. J. Human Pharmaceuticals in the Aquatic Environment: A Challenge to Green Chemisty. *Chem. Rev.* **2007**, *107* (6), 2319–2364.

(6) Linker, B. R.; Khatiwada, R.; Perdrial, N.; Abrell, L.; Sierra-Alvarez, R.; Field, J. A.; Chorover, J. Adsorption of Novel Insensitive Munitions Compounds at Clay Mineral and Metal Oxide Surfaces. *Environ. Chem.* **2015**, *12* (1), 74–84.

(7) Figueroa, R. A.; Mackay, A. A. Sorption of Oxytetracycline to Iron Oxides and Iron Oxide-Rich Soils. *Environ. Sci. Technol.* **2005**, *39* (17), 6664–6671.

(8) Han, H.; Rafiq, M. K.; Zhou, T.; Xu, R.; Mašek, O.; Li, X. A Critical Review of Clay-Based Composites with Enhanced Adsorption Performance for Metal and Organic Pollutants. *J. Hazard. Mater.* **2019**, *369* (February), 780–796.

(9) Nayak, P. S.; Singh, B. K. Removal of Phenol from Aqueous Solutions by

590 Sorption on Low Cost Clay. *Desalination* **2007**, *207* (1–3), 71–79.
591 (10) Cheng, W.; Elaheh, Lot, K.; Remi, M.; Hanna, K. Adsorption of Quinolone
592 Antibiotics to Goethite under Seawater Conditions : Application of a Surface
593 Complexation Model. *Environ. Sci. Technol.* **2019**, *53*, 1130–1138.
594 (11) Gao, J.; Pedersen, J. A. Adsorption of Sulfonamide Antimicrobial Agents to Clay
595 Minerals. *Environ. Sci. Technol.* **2005**, *39* (24), 9509–9516.
596 (12) Sheng, F.; Ling, J.; Wang, C.; Jin, X.; Gu, X.; Li, H.; Zhao, J.; Wang, Y.; Gu, C.
597 Rapid Hydrolysis of Penicillin Antibiotics Mediated by Adsorbed Zinc on Goethite
598 Surfaces. *Environ. Sci. Technol.* **2019**, *53* (18), 10705–10713.
599 (13) Gu, B.; Mehlhorn, T. L.; Liang, L.; McCarthy, J. F. Competitive Adsorption,
600 Displacement, and Transport of Organic Matter on Iron Oxide: I. Competitive
601 Adsorption. *Geochim. Cosmochim. Acta* **1996**, *60* (11), 1943–1950.
602 (14) Gu, B.; Mehlhorn, T. L.; Liang, L.; Mccarthy, J. F. Competitive Adsorption ,
603 Displacement , and Transport of Organic Matter on Iron Oxide: II. Displacement and
604 Transport. *Geochim. Cosmochim. Acta* **1996**, *60* (16), 2977–2992.
605 (15) Liu, S. Cooperative Adsorption on Solid Surfaces. *J. Colloid Interface Sci.* **2015**,
606 *450*, 224–238.
607 (16) Evanko, C. R.; Dzombak, D. A. Surface Complexation Modeling of Organic
608 Acid Sorption to Goethite. *J. Colloid Interface Sci.* **1999**, *206*, 189–206.
609 (17) Hanna, K.; Boily, J. F. Sorption of Two Naphthoic Acids to Goethite Surface
610 under Flow through Conditions. *Environ. Sci. Technol.* **2010**, *44* (23), 8863–8869.
611 (18) Xu, J.; Marsac, R.; Wei, C.; Wu, F.; Boily, J. F.; Hanna, K. Cobinding of

612 Pharmaceutical Compounds at Mineral Surfaces: Mechanistic Modeling of Binding
613 and Cobinding of Nalidixic Acid and Niflumic Acid at Goethite Surfaces. *Environ.*
614 *Sci. Technol.* **2017**, *51* (20), 11617–11624.
615 (19) Xu, J.; Marsac, R.; Costa, D.; Cheng, W.; Wu, F.; Boily, J. F.; Hanna, K.
616 Co-Binding of Pharmaceutical Compounds at Mineral Surfaces: Molecular
617 Investigations of Dimer Formation at Goethite/Water Interfaces. *Environ. Sci.*
618 *Technol.* **2017**, *51* (15), 8343–8349.
619 (20) Cheng, W.; Zhou, L.; Marsac, R.; Boily, J. F.; Hanna, K. Effects of Organic
620 Matter–Goethite Interactions on Reactive Transport of Nalidixic Acid: Column Study
621 and Modeling. *Environ. Res.* **2020**, *191*, 110187.
622 (21) Gu, C.; Karthikeyan, K. G. Sorption of the Antimicrobial Ciprofloxacin to
623 Aluminum and Iron Hydrous Oxides. *Environ. Sci. Technol.* **2005**, *39* (23),
624 9166–9173.
625 (22) Haderlein, S. B.; Weissmahr, K. W.; Schwarzenbach, R. P. Specific Adsorption
626 of Nitroaromatic Explosives and Pesticides to Clay Minerals. *Environ. Sci. Technol.*
627 **1996**, *30* (2), 612–622.
628 (23) Yang, Y.; Duan, J.; Jing, C. Molecular-Scale Study of Salicylate Adsorption and
629 Competition with Catechol at Goethite/Aqueous Solution Interface. *J. Phys. Chem. C*
630 **2013**, *117* (20), 10597–10606.
631 (24) Shakiba, S.; Hakimian, A.; Barco, L. R.; Louie, S. M. Dynamic Intermolecular
632 Interactions Control Adsorption from Mixtures of Natural Organic Matter and Protein
633 onto Titanium Dioxide Nanoparticles. *Environ. Sci. Technol.* **2018**, *52* (24),

14158–14165.

(25) Kretzschmar, R.; Robarge, W. P.; Amoozegar, A. Influence of Natural Organic Matter on Colloid Transport through Saprolite. *Water Resour. Res.* **1995**, *31* (3), 435–445.

(26) Cornell, R. M.; Schwertmann, U. *The Iron Oxides: Structure, Properties, Reactions, Occurrences and Uses*; 2003.

(27) Rusch, B.; Hanna, K.; Humbert, B. Coating of Quartz Silica with Iron Oxides: Characterization and Surface Reactivity of Iron Coating Phases. *Colloids Surfaces A Physicochem. Eng. Asp.* **2010**, *353* (2–3), 172–180.

(28) Hanna, K.; Martin, S.; Quilès, F.; Boily, J.-F. Sorption of Phthalic Acid at Goethite Surfaces under Flow-Through Conditions. *Langmuir* **2014**, *30* (23), 6800–6807.

(29) McKnlght, D. M.; Aiken, G. R.; Thorn, K. A.; Bencala, K. E.; Zellweger, G. W.; Feder, G. L. Sorption of Dissolved Organic Carbon by Hydrous Aluminum and Iron Oxides Occurring at the Confluence of Deer Creek with the Snake River, Summit County, Colorado. *Environ. Sci. Technol.* **1992**, *26* (7), 1388–1396.

(30) Helbling, E. W.; Zagarese, H. Photochemistry of Chromophoric Dissolved Organic Matter in Natural Waters. In *UV Effects in Aquatic Organisms and Ecosystems*; 2003; 185–219.

(31) Pokharel, R.; Li, Q.; Zhou, L.; Hanna, K. Water Flow and Dissolved Mn(II) Alter Transformation of Pipemidic Acid by Manganese Oxide. *Environ. Sci. Technol.* **2020**, *54* (13), 8051–8060.

(32) Zhou, L.; Martin, S.; Cheng, W.; Lassabatere, L.; Boily, J. F.; Hanna, K. Water Flow Variability Affects Adsorption and Oxidation of Ciprofloxacin onto Hematite. *Environ. Sci. Technol.* **2019**, *53* (17), 10102–10109.

(33) Yiacoumi, S.; Tien, C. Modeling Adsorption of Metal Ions from Aqueous Solutions. I. Reaction-Controlled Cases. *Journal of Colloid And Interface Science*. 1995, pp 333–346.

(34) Axe, K.; Persson, P. Time-Dependent Surface Speciation of Oxalate at the Water-Boehmite (γ-AIOOOH) Interface: Implications for Dissolution. *Geochim. Cosmochim. Acta* **2001**, *65* (24), 4481–4492.

(35) Zhou, L.; Cheng, W.; Marsac, R.; Boily, J.-F.; Hanna, K. Silicate Surface Coverage Controls Quinolone Transport in Saturated Porous Media. *J. Colloid Interface Sci.* **2021**, 607, 347-356.

(36) Nkedi-Kizza, P.; Shinde, D.; Savabi, M. R.; Ouyang, Y.; Nieves, L. Sorption Kinetics and Equilibria of Organic Pesticides in Carbonatic Soils from South Florida. *J. Environ. Qual.* **2006**, *35* (1), 268–276.

(37) David, L. P.; Appelo, C. A. J. User's Guide to PHREEQC (Version 2)— A Computer Program for Speciation, Batch-Reaction, One-Dimensional Transport, and Inverse Geochemical Calculations; 1995.

(38) Brusseau, M. L.; Gerstl, Z.; Augustijn, D.; Rao, P. S. C. Simulating Solute Transport in an Aggregated Soil with the Dual-Porosity Model: Measured and Optimized Parameter Values. *J. Hydrol.* **1994**, *163* (1–2), 187–193.

(39) Šimůnek, J.; van Genuchten, M. T. Modeling Nonequilibrium Flow and

Transport Processes Using HYDRUS. *Vadose Zo. J.* **2008**, *7* (2), 782–797.

(40) Cheng, W.; Hanna, K.; Boily, J. F. Water Vapor Binding on Organic Matter-Coated Minerals. *Environ. Sci. Technol.* **2019**, *53* (3), 1252–1257.

(41) Kleber, M.; Sollins, P.; Sutton, R. A Conceptual Model of Organo-Mineral Interactions in Soils: Self-Assembly of Organic Molecular Fragments into Zonal Structures on Mineral Surfaces. *Biogeochemistry* **2007**, *85* (1), 9–24.

(42) Coward, E. K.; Ohno, T.; Sparks, D. L. Direct Evidence for Temporal Molecular Fractionation of Dissolved Organic Matter at the Iron Oxyhydroxide Interface. *Environ. Sci. Technol.* **2019**, *53* (2), 642–650.